



Thermal evolution of spin excitations in honeycomb Ising antiferromagnetic FePSe_3



Lebing Chen^{1,2,3}✉, Xiaokun Teng³, Ding Hu⁴, Feng Ye⁵, Garrett E. Granroth⁵, Ming Yi³, Jae-Ho Chung⁶✉, Robert J. Birgeneau^{1,2}✉ & Pengcheng Dai³✉

We use elastic and inelastic neutron scattering (INS) to study the antiferromagnetic (AF) phase transitions and spin excitations in the two-dimensional (2D) zig-zag antiferromagnet FePSe_3 . By determining the magnetic order parameter across the AF phase transition, we conclude that the AF phase transition in FePSe_3 is first-order in nature. In addition, our INS measurements reveal that the spin waves in the AF ordered state have a large easy-axis magnetic anisotropy gap, consistent with an Ising Hamiltonian, and possible biquadratic magnetic exchange interactions. On warming across T_N , we find that dispersive spin excitations associated with three-fold rotational symmetric AF fluctuations change into FM spin fluctuations above T_N . These results suggest that the first-order AF phase transition in FePSe_3 may arise from the competition between C_3 symmetric AF and C_1 symmetric FM spin fluctuations around T_N , in place of a conventional second-order AF phase transition.

Two-dimensional (2D) spin models are one of the most well-studied magnetic systems in condensed matter physics. The pioneering solution by Onsager in 1944¹ revealed that the 2D ferromagnetic (FM) Ising model, characterized by nearest neighbor coupling J , undergoes a magnetic phase transition at $k_B T_C = 2.269J$, exhibiting an order parameter critical exponent $\beta = 1/8$. The 2D XY model, on the other hand, lacks long-range order, but it exhibits the ability to undergo a Berezinskii-Kosterlitz-Thouless transition, during which the correlation function transitions from an exponential decay to a power-law behavior as a function of distance^{2,3}. In real magnetic materials, spins exhibit free 3D rotation rather than adhering to binary orientations or 2D rotations, and the Hamiltonian for actual magnetic systems will take the form of a Heisenberg model plus magnetic anisotropy⁴. According to the Mermin-Wagner theorem, in the case of an isotropic Heisenberg Hamiltonian with short-range magnetic exchange couplings, the thermal fluctuations are strong enough to prevent long-range magnetic order in the 2D limit at any finite temperature⁵, with the correlation length diverging only at absolute zero. Conversely, in the presence of easy-axis/easy-plane anisotropy, the renormalization group flow will favor the selection of the anisotropic component of the Hamiltonian as the relevant parameter, resulting in critical behavior that aligns with predictions from the Ising/XY models⁶.

The discovery of long-range magnetic order at non-zero temperatures in the 2D monolayer of several honeycomb lattice van der Waals (vdW) ferromagnets and antiferromagnets suggests a suppression of the thermal fluctuations, most likely due to the formation of an Ising-type magnetic anisotropy gap in these materials^{7–12}. To understand the microscopic origin of the long-range magnetic order in the 2D limit for different classes of vdW materials, it is therefore important to determine the magnetic properties of their 3D bulk compounds. While the FM Ising Hamiltonian on a 2D square lattice has been solved¹, the situation for Ising spin systems in 2D honeycomb lattices is more complicated. As a non-Bravais lattice, the honeycomb structure can host a few different collinear magnetic structures, including simple ferromagnets, Néel antiferromagnet with c -axis aligned moments, stripy antiferromagnet, and zig-zag antiferromagnet [Fig. 1e], depending on the relative strengths of nearest J_1 (NN), next nearest J_2 (NNN), and next-next nearest neighbor J_3 (NNNN) magnetic exchange interactions [Fig. 1a]¹³. The first two magnetic structures have the same in-plane ordering wavevectors as the lattice vectors, and respect the three-fold rotational (C_3) symmetry of the honeycomb lattice. The stripy and zig-zag antiferromagnetic (AF) structures, however, break the C_3 rotational symmetry of the honeycomb lattice to C_1 and fold the first Brillouin zone (FBZ) into a smaller rectangular magnetic FBZ. In these structures, there will be three

¹Department of Physics, University of California, Berkeley, CA 94720, USA. ²Material Sciences Division, Lawrence Berkeley National Laboratory, Berkeley, CA 94720, USA. ³Department of Physics and Astronomy, Rice University, Houston, TX 77005, USA. ⁴School of Physics, Hangzhou Normal University, Hangzhou, Zhejiang 311121, China. ⁵Neutron Scattering Division, Oak Ridge National Laboratory, Oak Ridge, TN 37831, USA. ⁶Department of Physics, Korea University, Seoul 02841, Korea. ✉e-mail: lebingchen@berkeley.edu; jaehc@korea.ac.kr; robertjb@berkeley.edu; pdai@rice.edu

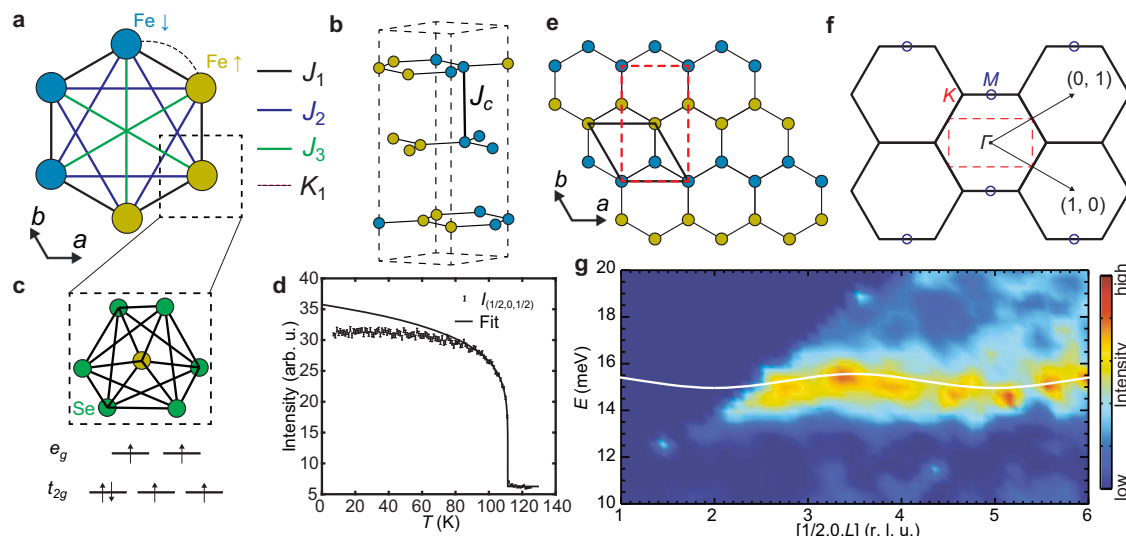


Fig. 1 | Real/reciprocal space of FePSe₃ and spin waves along in-plane and *c*-axis directions. **a** Schematics of the intralayer AF magnetic structure and exchange interactions. **b** Interlayer magnetic structure and coupling J_c . **c** Local Fe²⁺ environment in FePSe₃, with the 3d⁶ spin configuration in an octahedral environment. **d** Neutron intensity of magnetic Bragg peak (1/2 0 1/2) as a function of temperature. **e** The in-plane zig-zag magnetic structure. The bold black rhombus shows the lattice

unit cell and the dashed red rectangle shows the magnetic unit cell. **f** The reciprocal space with black hexagons shows the lattice FBZ and the dashed red rectangle shows the magnetic FBZ. The blue dots are the magnetic Bragg peaks from the magnetic structure shown in (e). **g** Out-of-plane spin wave dispersion along [1/2 0 L] from the experiment. All error bars indicate one standard deviation.

magnetic domains separated by 60°, meaning that the overall magnetism still obeys the underlying C_3 lattice symmetry. The magnetic order parameter is not a direct measure of the ordered or staggered moment because it has multiple components. For example, the order parameter for the zig-zag AF order is composed of three components (Ψ_1, Ψ_2, Ψ_3), each reflecting the staggered moment along one of the three C_3 axes¹⁴. By probing the static magnetic order and spin excitations across the magnetic phase transition, one can obtain information concerning the behaviors of the phase transition and compare the results with the expectations of the conventional Ising or XY models.

For the FM honeycomb system CrSiTe₃, the critical behavior of the magnetic phase transition exhibits 2D Ising characteristics^{15,16}, with a dimensional crossover from 2D to 3D near T_C ¹⁷. For other honeycomb lattice ferromagnets such as CrI₃, VI₃, and CrGeTe₃, the critical behavior is more reminiscent of the tricritical mean field model^{18–22}. For AF-ordered MnPS₃, NiPS₃, and CoPS₃, the critical behavior near T_N shows 3D XY or Ising characteristics^{23–25}. However, none of these AF materials with Ising-type anisotropy follow the genuine 2D Ising model due to the limited strength of the anisotropy, along with interlayer interactions that impact the magnetic phase transition^{26,27}.

FePS₃ and FePSe₃ constitute a potential material family for exploring an Ising-type antiferromagnetic phase transition accompanied by C_3 symmetry breaking. This study specifically centers on FePSe₃ [Fig. 1a, c]. FePSe₃ belongs to the rhombohedral $R\bar{3}$ space group, with hexagonal layers stacked through weak vdW interactions along the *c*-axis [Fig. 1b]²⁸. Compared with FePS₃ in the monoclinic $C/2m$ symmetry group, FePSe₃ preserves the C_3 symmetry and therefore is ideal to study any possible magnetic order induced in-plane C_3 symmetry breaking without significant interlayer coupling effects²⁹. Since FePSe₃ has an in-plane zig-zag AF structure below $T_N = 110$ K, we expect an FM exchange interaction J_1 between NN, and AF exchange interactions in J_2 and J_3 between NNN and NNNN, respectively [Fig. 1a]²⁸. In the 3D bulk limit, the AF ordering wavevector is $\mathbf{Q}_{AF} = (1/2, 0, 1/2)$ [Fig. 1b, f] due to a weak AF interlayer coupling J_c [Fig. 1b]²⁸. The magnetic Fe²⁺ ion has a 3d⁶ electronic orbital with four unpaired spins, giving $S = 2$. A strong spin-orbit coupling (SOC) induces a large magnetic anisotropy with the *c*-axis as the easy axis^{28,30}. Raman scattering experiments on bulk and monolayer FePSe₃ have observed a ~15 meV spin gap, suggesting that the system is Ising-like^{11,12}.

In this work, we use elastic and inelastic neutron scattering (INS) to study the magnetic order and spin dynamics in bulk single crystal FePSe₃. The temperature dependence of the magnetic order parameter from elastic neutron scattering experiments suggests that the AF phase transition is first-order in nature [Fig. 1d]. In the AF ordered state, our INS experiments reveal that spin waves are gapped below ~15 meV, consistent with Raman scattering results^{11,12}, and are highly 2D with weak dispersion along the *c*-axis [Fig. 1g]. By fitting the spin-wave dispersion spectra using linear spin wave theory (LSWT)³¹, we determine magnetic exchange couplings, magnetic anisotropy, and find evidence for a biquadratic term in the spin Hamiltonian. On warming above T_N , we find dispersive spin excitations that can be explained by AF and FM excitations from honeycomb lattice clusters with the C_3 symmetry. These results are different from the expectation of a conventional AF second-order phase transition, suggesting that the long-range AF order in FePSe₃ is replaced by C_3 magnetic honeycomb lattice clusters as the temperature is raised above T_N . The uncorrelated paramagnetic scattering from individual Fe ions is only established at temperatures well above T_N .

Results

Neutron diffraction experiments

Single crystal neutron diffraction experiments are performed at 6 K and 125 K to refine crystal and magnetic structures. From neutron diffraction experiments, the magnetic ordering wavevector observed at $\mathbf{Q}_{AF} = (1/2, 0, 1/2)$ as well as the refinement at 6 K (see Supplementary Fig. 2) confirms the zig-zag magnetic structure, and the temperature dependence of the order parameter is shown in Fig. 1d. A power law fit of the order parameter with $I = I_0(1 - (T/T_N)^{2\beta})$ yields a critical exponent $\beta = 0.063$, which is much smaller than the 2D Ising model prediction $\beta = 1/8$, suggesting a first-order nature of the phase transition. This is further supported by measurements of correlation lengths which jump abruptly at T_N ³⁰.

INS experiments and linear spin wave theory fits

Figures 1g and 2b show the measured spin wave dispersions of FePSe₃ at 5 K along the *c* axis and within the 2D honeycomb lattice plane, respectively. The overall dispersion has a band top of ~40 meV, with an anisotropy gap of ~15 meV at the Γ and M points. The large anisotropy gap value is also observed in the sister compound FePS₃, which is due to the combined effects

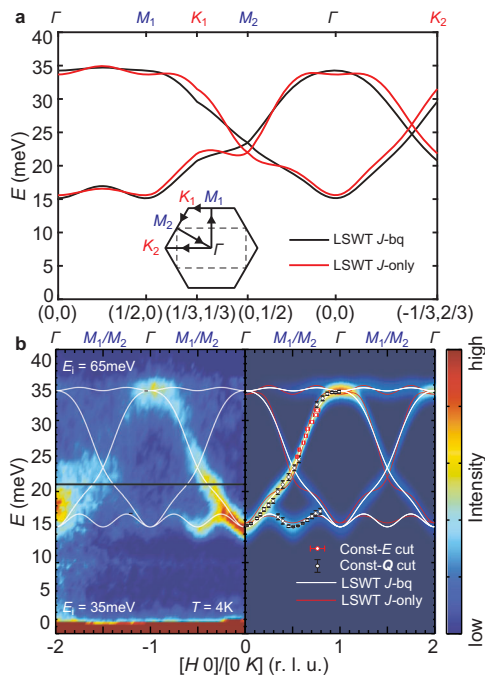


Fig. 2 | Spin waves in FePSe₃. **a** Calculated spin wave dispersion with (black) and without (red) biquadratic interactions. The inset shows the **Q** scan path. **b** LSWT fit of the experimental data with (white) and without (red) biquadratic interactions. All error bars indicate one standard deviation.

of SOC in the 3d⁶ orbital of Fe²⁺ and the distortion of the FeSe₆ octahedron [Fig. 1c]. For comparison, the isostructural compounds MnPSe₃ and MnPS₃ do not exhibit such large gaps because their 3d⁵ electrons have quenched orbital moments^{26,32}. The spin waves propagating along the *c*-axis exhibit significantly less dispersion in contrast to the in-plane spin waves, featuring a bandwidth of ~1 meV for the former as opposed to a 20 meV bandwidth for the latter, indicating the presence of a very weak interlayer coupling *J_c* [Fig. 1g]. This is consistent with the fact that the *T_N* of FePSe₃ changes little as a function of layer numbers, suggesting that the interlayer exchange interactions have minimal effect on the magnetic phase transition in FePSe₃^{9,11}.

To describe the in-plane spin wave dispersion, we first use LSWT to calculate the spin waves with the spin Hamiltonian

$$H_0 = \sum_{\langle i,j \rangle} J_{ij} \mathbf{S}_i \cdot \mathbf{S}_j + \sum_i D_z (S_i^z)^2 \quad (1)$$

where the bilinear (Heisenberg) exchange interaction *J_{ij}* is summed over the 1st, 2nd, and 3rd NN, and *D_z* is the single-ion anisotropy with the *z*-axis as its easy axis. It is worth noting that within the actual system, magnetic anisotropy may stem from either single-ion effects or Ising-type exchanges. Therefore, the Hamiltonian can encompass Ising exchange terms *J_zS_{iz}S_{jz}* in addition to the single-ion anisotropy. Nevertheless, within the framework of linear spin wave theory, the Ising term's impact on dispersion will be identical to that of single-ion anisotropy, provided that the respective parameters are appropriately adjusted³³ (see Supplementary Table III). For the sake of simplicity, we have chosen to solely include the single-ion anisotropy term here. Using a least-square-error fitting method with *S* = 2, we extract the magnetic exchange coupling parameters as shown in Table 1. However, the best fitting using this model with uniform *J₁* does not precisely reproduce the measured dispersion, especially the low-energy part perpendicular to the zig-zag direction. In fact, the exact same scenario is observed in the sister compound FePS₃³⁴ where a simple Heisenberg model plus anisotropy cannot account for the spin excitations accurately. In the case of FePS₃, two approaches have been utilized to resolve this problem,

Table 1 | Magnetic exchange interaction strength in different models in FePSe₃

Model	<i>J₁</i>	<i>J₂</i>	<i>J₃</i>	<i>K₁</i>	<i>D_z</i>
Uniform <i>J₁</i>	-2.30	-0.23	2.01	0	-2.74
<i>J_{1a}</i> - <i>J_{1b}</i>	-2.26/-0.72	0.09	1.28	0	-2.45
<i>J₁</i> -bq	-1.32	0.12	1.28	-0.22	-2.31

All units in meV. In the *J_{1a}*-*J_{1b}* model, the *J_{1a}* indicates FM interactions in the zig-zag chain, and *J_{1b}* indicates interactions between chains. *J₁*, *J₂*, *J₃* indicate the first, second, and third nearest neighbor Heisenberg exchange, respectively. *K₁* refers to the nearest-neighbor biquadratic interactions, and *D_z* stands for single-ion anisotropy.

and here we apply them to FePSe₃ as well. The first is to introduce bond-dependent *J₁* with *J_{1a}* bonding the parallel spins and *J_{1b}* for anti-parallel spins; The second is to introduce a biquadratic interaction

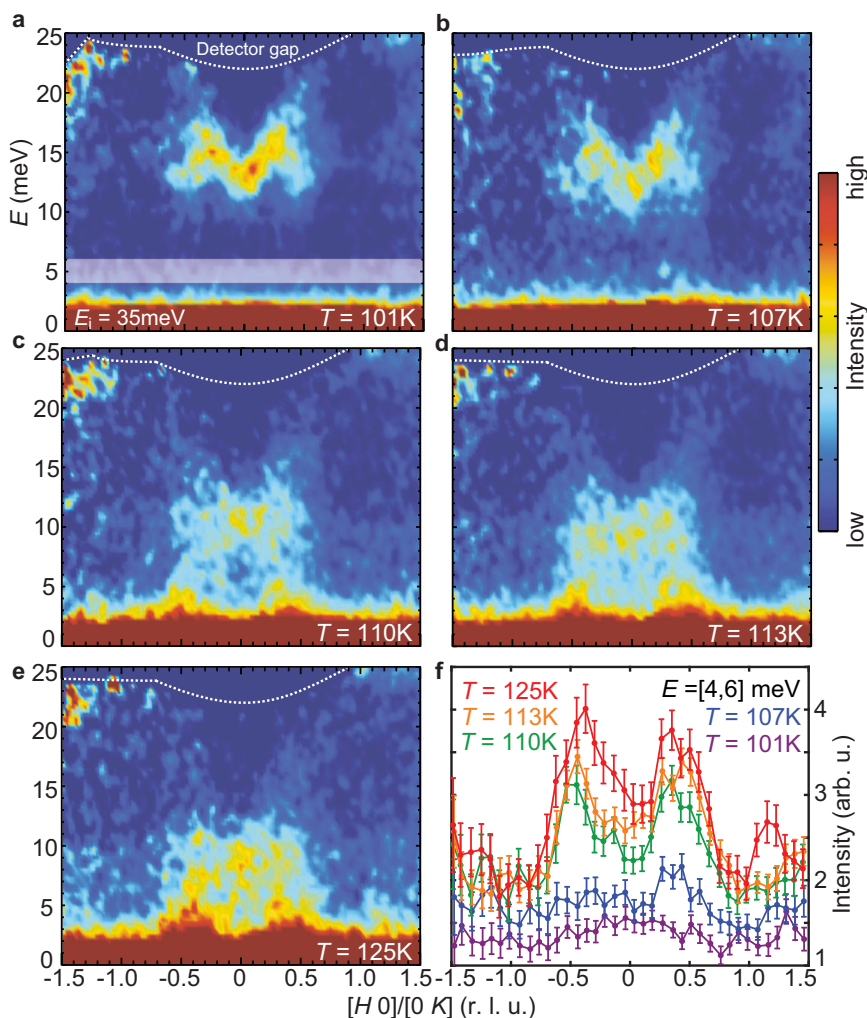
$$H = H_0 + \sum_{\langle i,j \rangle} K_{ij} (\mathbf{S}_i \cdot \mathbf{S}_j)^2 \quad (2)$$

where the biquadratic exchange *K_{ij}* is summed over the 1st NN only. Both methods stabilize the zig-zag AF order, and with proper fitting parameters in Table 1, they yield nearly identical dispersions that can accurately reproduce the experimental data. For the *J_{1a}*-*J_{1b}* model, the difference between *J_{1a}* and *J_{1b}* is large, indicating that a lattice distortion should accompany the magnetic phase transition as in the case of FePS₃. However, no obvious lattice parameter change is observed across *T_N*, indicating that the *J_{1a}*-*J_{1b}* model is unlikely to be correct (see Supplementary Fig. 3 and Fig. 4). On the other hand, The existence of a biquadratic interaction has been theoretically proposed in many such 2D magnetic systems with edge-shared octahedron structures^{35,36}, and therefore may be the more suitable model for describing the spin waves in FePSe₃. The situation is similar in the case of iron-based superconductors, where a biquadratic interaction has been used to account for the observed in-plane spin wave dispersions^{37,38}. A noteworthy fact is that the low-energy magnons at the Γ point are linearly coupled to phonons, which introduces a magnon-polaronic gap that lifts the twofold degeneracy of the AF magnons^{11,12}. This suggests the necessity of introducing a magnon-phonon coupling term into the spin Hamiltonian. However, the impact of this term is minimal, exhibiting a gap of ~0.6 meV, a value below the resolution of the instruments. Hence, it is omitted from equation (2). Furthermore, the required strength of the Kitaev interaction (0.03 meV) to induce the magnon-phonon gap is significantly less than that of the Heisenberg exchanges, and thus, these are not taken into account in the fitting parameters.

Thermal evolution of the spin excitations

The first-order nature of the AF phase transition also displays itself in the spin fluctuations in the neighborhood of *T_N*. Figure 3 shows a summary of the INS spectrum near *T_N* = 110 K. At *T* = 101 K, in-plane spin excitations are well-defined and similar to spin waves at 5 K [Fig. 3a]. On warming to *T* = 107 K, spin excitations remain well defined, but become broader with an anisotropy spin gap above 10 meV (Fig. 3b). Upon further warming to 110 K, the spin gap drastically decreases to zero at the *M* point, while keeping a non-zero value at the Γ point [Fig. 3c]. A cut along the [*H*, 0] direction at *E* = 5 ± 1 meV shows clearly that the *M* point spin fluctuations are enhanced from 110 K to 125 K, different from the expectation of critical magnetic scattering associated with a second-order phase transition. Although the spin gap closing at the *M* point may arise from the vanishing static magnetic moment across *T_N*, the differences in the temperature dependence of the spin gap at Γ and *M* points cannot be explained by a second-order AF phase transition since the Γ and *M* points are equivalent within the spin wave theory which requires long-range AF order and folding of the Brillouin zone below *T_N*. This is consistent with the observed first-order transition in the AF order parameter [Fig. 1d]. In the paramagnetic state, the rectangular magnetic Brillouin zone unfolds to the hexagonal

Fig. 3 | Spin excitations in FePSe₃ at different temperatures. Spin excitations in FePSe₃ in (a) 101 K, (b) 107 K, (c) 110 K, (d) 113 K, and (e) 125 K. f A constant-*E* cut of the intensity in (a–e) with *E* integrated between 4 and 6 meV. The incident neutron energy used here is *E_i* = 35 meV. All error bars indicate one standard deviation.



lattice Brillouin zone. However, we find similar spin excitations as in the AF-ordered state [Fig. 3d–f].

Discussion

Although the AF phase transition in FePSe₃ is first-order, the short-range zig-zag order may still persist near the phase transition. A natural way to reconcile the existence of the zig-zag order and the C₃ symmetry is to combine all the zig-zag domains with equal weight [Fig. 4a], while the size of the fluctuation domains determines the correlation lengths of the short-range order. To understand the nature of the dispersive paramagnetic spin excitations in FePSe₃, we plot constant-*E* slices in the [*H* *K*] plane at *E* = 5 ± 2 meV [Fig. 4c] and 11 ± 2 meV [Fig. 4d] at 110 K, which shows the spin excitations at the *M* points and their connections, respectively. The low-energy spin excitations show diffusive hexagonal patterns which are hollow at the Γ point, and the high-energy excitations show plate-like hexagonal patterns. Inspired by the spin cluster methods used in refs. 39–41, we apply a similar analysis on FePSe₃. Assuming that the spins form clusters of hexagons with zig-zag order [Fig. 4a], we calculate the neutron intensity *I*(**Q**) with

$$I(\mathbf{Q}) \propto f^2(\mathbf{Q}) \sum_{(m,n)} e^{i\mathbf{Q}(r_m - r_n)} \left(1 - \frac{Q_z^2}{Q^2}\right) \langle S_m^z S_n^z \rangle \quad (3)$$

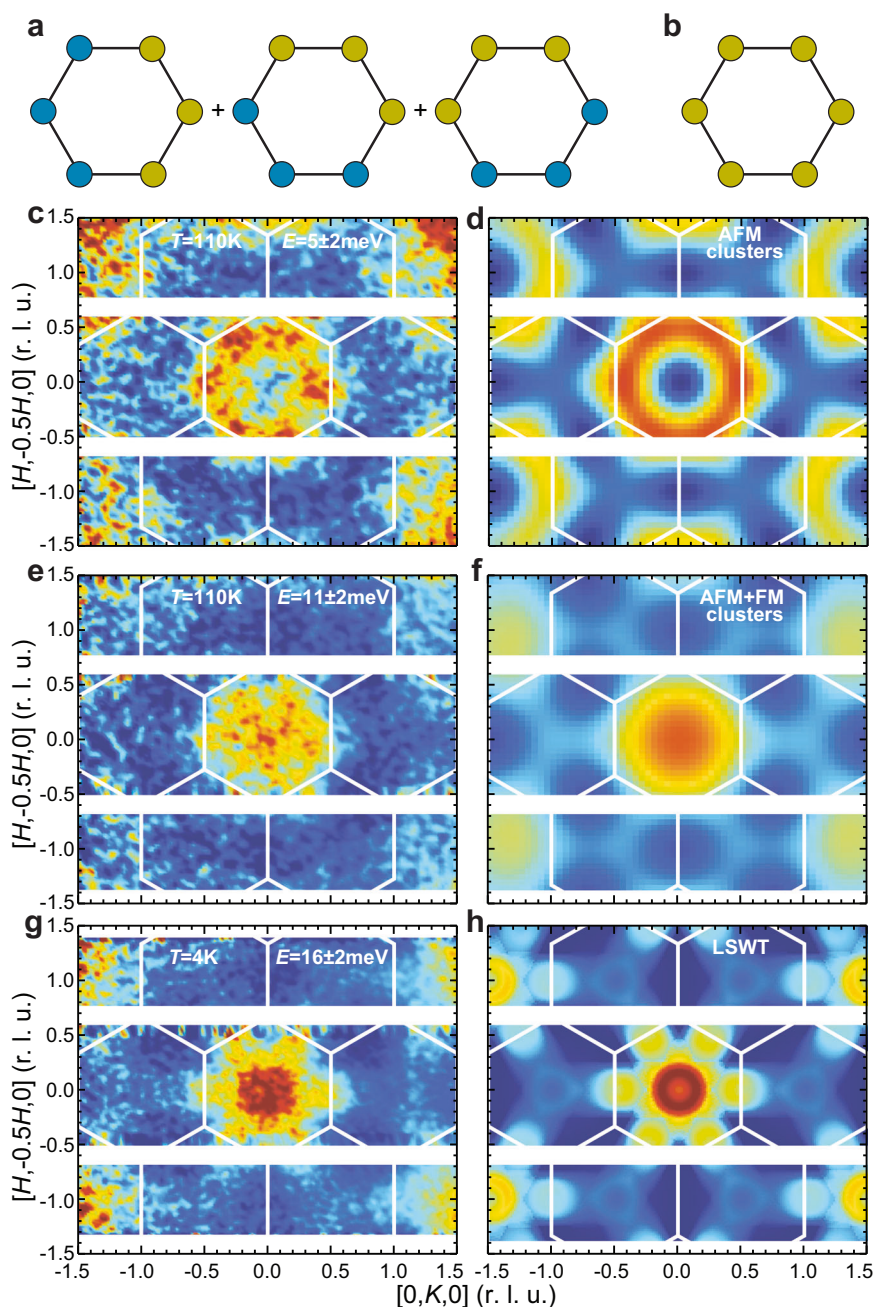
where *f*²(**Q**) is the magnetic form factor, *m*, *n* ∈ 1, ..., 6 is the index for spins in Fig. 4a and b. The calculated *I*(**Q**) is then averaged over six zig-zag spin configurations. Figure 4d, f shows the calculated intensity from the zig-zag

clusters [Fig. 4a], which matches well with the experimental result at low energy. For the higher energy part at 11 meV, due to the enhanced Γ point spin fluctuations, an additional FM cluster is required [Fig. 4b] in order to reconstruct the plate-like excitation pattern.

The spin fluctuations observed at 110 K encode substantial information regarding the spin correlations in FePSe₃. The pillar-like feature of the spin excitations at the *M* point in Fig. 3c indicates that the **Q**-dependence of low-energy spin excitations remains unchanged below ~8 meV. This implies that an integral over the low-energy excitations can reasonably approximate the instantaneous spin correlations. Consequently, despite our zig-zag cluster calculation is used to reproduce the spin fluctuation in the energy range *E* = [3, 7] meV, it is reasonable to infer that this zig-zag arrangement effectively reflects the nature of these instantaneous spin correlations.

A noteworthy observation is that even in the AF state at 4 K, the dynamical spin-spin correlation centers around the FM wavevector located at Γ , rather than the AF wavevector at *M* [Fig. 4g, h]. The reason is that as the magnetic anisotropy grows, the AF spin wave excitations are gradually replaced by local spin-flip excitations. In an isotropic AF Heisenberg model, the magnetic excitations are spin waves that give zero structure factor at the FM wavevector, while in a pure AF Ising model, the spin-flip excitations will introduce a non-zero intensity centered at the Γ point. In the case of FePSe₃, the robust magnetic anisotropy shifts the primary spin excitations from AF spin waves to spin-flip excitations. As the temperature rises to *T_N*, the local spin-flip excitation remains gapped, indicating that the dynamic susceptibility associated with spin-flip scattering remains non-zero. Consequently,

Fig. 4 | Simulation on spin fluctuations at Néel temperature in FePSe₃. **a, b** Zig-zag AF and FM clusters were used to simulate the spin fluctuation, respectively. **c** Experimental data at $T = 110$ K and $E = [3,7]$ meV. **d** Calculated neutron intensity of the AF cluster in **(a)**. **e** Experimental data at $T = 110$ K and $E = [9,13]$ meV. **f** Calculated neutron intensity of the AF cluster **(a)** plus the FM cluster **(b)**. The AF clusters and FM clusters are weighted with a ratio of 2:1 in **(f)**. **g** Experimental data at $T = 4$ K and $E = [14,18]$ meV. **h** Calculated neutron intensity at the same energy range as **(g)** by LSWT with parameters from Table 1.



it cannot be the primary driving force behind the first-order magnetic phase transition. Instead, the excitations of zig-zag clusters at T_N become gapless, implying that the dominant component of spin configurations near T_N is the zig-zag short-range order. It can be speculated that the magnetic phase transition is driven by a discontinuous condensation of these zig-zag hexagonal clusters, corresponding to the C_3 - C_1 symmetry breaking. This distinguishes it from the fluctuations observed in conventional Ising magnets that break the Z_2 time-reversal symmetry through spin-flip scatterings.

In summary, we utilized neutron scattering to study the spin excitations and spin fluctuations in FePSe₃ across T_N . By analyzing the spin wave dispersion, we find evidence for biquadratic magnetic exchange interactions in the effective spin Hamiltonian terms. The microscopic origin of the biquadratic term remains to be determined. In addition, our magnetic order parameter measurements indicate that the AF phase transition is first-order in nature. From measurements of the temperature-dependent spin excitations across T_N , we infer that the AF phase transition may be driven by the C_3

to C_1 symmetry breaking from low-energy spin clusters associated with zig-zag AF honeycomb lattice. Our results provide an enriched perspective on the intricate interplay between magnetic interactions and structural symmetries in the Ising magnetic systems with additional C_3 symmetry breaking.

Methods

Sample synthesis and the reciprocal lattice

Single crystals of FePSe₃ were synthesized using the chemical vapor transport method described in ref. 42. Around 2g stoichiometric starting materials (Fe, P, Se) were sealed in a quartz tube together with around 0.1 g iodine as a transport agent. The tube was then kept in a tube furnace for a week with a temperature gradient from 650 °C to 600 °C. FePSe₃ flakes were collected at the cold end of the tube with typical masses of 5–10 mg. The momentum transfer Q is referenced in reciprocal lattice units with respect to the hexagonal unit cell of FePSe₃ with $a = b = 6.26$ Å, $c = 19.71$ Å. The high symmetry points Γ , M , K in the reciprocal space are specified in Fig. 1f.

Neutron diffraction

Neutron diffraction experiments were performed at the CORELLI spectrometer at the Spallation Neutron Source, Oak Ridge National Laboratory⁴³ on a single crystal sample. The overall diffraction patterns were collected at 6 K and 125 K. Order parameter scans were then performed at the (1/2 0 1/2) magnetic Bragg peak together with scans on the (3 0 0) and (3 3 0) Bragg peak which track the temperature dependence of the lattice parameters. The data collected at CORELLI was used to refine the crystallographic parameters through the JANA2006 software⁴⁴ (See Supplementary Tables I and II).

Inelastic neutron scattering

Inelastic neutron scattering experiments were performed at the ARCS spectrometer⁴⁵ on ~0.5 g of co-aligned crystals at the Spallation Neutron Source, Oak Ridge National Laboratory. The inelastic neutron spectra were plotted using DAVE-Mslice⁴⁶. For linear spin wave theory fitting, we utilized the SpinW package⁴⁷ to reconstruct the neutron structure factor $S(\mathbf{Q}, E)$. The gradient descent method was used to extract the best-fitting parameters.

Data availability

The data and code that support the plots within this paper and other findings of this study are available from the corresponding authors upon reasonable request.

Received: 28 November 2023; Accepted: 20 April 2024;

Published online: 13 May 2024

References

- Onsager, L. Crystal statistics. I. A two-dimensional model with an order-disorder transition. *Phys. Rev.* **65**, 117 (1944).
- Berezinskii, V. L. Destruction of long-range order in one-dimensional and two-dimensional systems having a continuous symmetry group I. Classical systems. *Sov. Phys. JETP* **32**, 493–500 (1970).
- Kosterlitz, J. M. & Thouless, D. J. Ordering, metastability and phase transitions in two-dimensional systems. *J. Phys. C: Solid State Phys.* **6**, 1181–1203 (1973).
- Gibertini, M., Koperski, M., Morpurgo, A. F. & Novoselov, K. S. Magnetic 2D materials and heterostructures. *Nat. Nano.* **14**, 408 (2019).
- Mermin, N. D. & Wagner, H. Absence of ferromagnetism or antiferromagnetism in one- or two-dimensional isotropic Heisenberg models. *Phys. Rev. Lett.* **17**, 1133 (1966).
- Goldenfeld, N. Lectures on Phase Transitions and the Renormalization Group. (CRC Press, Boca Raton, FL, 2018).
- Huang, B. et al. Layer-dependent ferromagnetism in a Van der Waals crystal down to the monolayer limit. *Nature* **546**, 270 (2017).
- Gong, C. et al. Discovery of intrinsic ferromagnetism in two-dimensional Van der Waals crystals. *Nature* **546**, 265 (2017).
- Lee, Jae-Ung. et al. Ising-type magnetic ordering in atomically thin FePS₃. *Nano Lett.* **16**, 7433–7438 (2016).
- Lee, Y. et al. Giant magnetic anisotropy in the atomically thin van der Waals Antiferromagnet FePS₃. *Adv. Electron. Mater.* **9**, 2200650 (2023).
- Luo, J. et al. Evidence for topological magnon-phonon hybridization in a 2D antiferromagnet down to the monolayer limit. *Nano Lett.* **23**, 2023–2030 (2023).
- Cui, J. et al. Chirality selective magnon-phonon hybridization and magnon-induced chiral phonons in a layered zigzag antiferromagnet. *Nat. Commun.* **14**, 3396 (2023).
- Fouet, J. B., Sindzingre, P. & Lhuillier, C. An investigation of the quantum J_1 - J_2 - J_3 model on the honeycomb lattice. *Eur. Phys. J. B* **20**, 241–254 (2001).
- Domany, E. & Riedel, E. K. Phase transitions in two-dimensional systems. *J. Appl. Phys.* **49**, 1315–1320 (1978).
- Liu, B. et al. Critical behavior of the quasi-two-dimensional semiconducting ferromagnet CrSiTe₃. *Sci. Rep.* **6**, 33873 (2016).
- Williams, T. J. et al. Magnetic correlations in the quasi-two-dimensional semiconducting ferromagnet CrSiTe₃. *Phys. Rev. B* **92**, 144404 (2015).
- Ron, A. et al. Dimensional crossover in a layered ferromagnet detected by spin correlation-driven distortions. *Nat. Commun.* **10**, 1654 (2019).
- Liu, Y. & Petrovic, C. Three-dimensional magnetic critical behavior in CrI₃. *Phys. Rev. B* **97**, 014420 (2018).
- Chen, L. et al. Magnetic anisotropy in ferromagnetic CrI₃. *Phys. Rev. B* **101**, 134418 (2020).
- Liu, Y., Abeykoon, M. & Petrovic, C. Critical behavior and magnetocaloric effect in VI₃. *Phys. Rev. Res.* **2**, 013013 (2020).
- Hao, Y. et al. Magnetic order and its interplay with structure phase transition in van der Waals ferromagnet VI₃. *Chin. Phys. Lett.* **38**, 096101 (2021).
- Lin, G. T. et al. Tricritical behavior of the two-dimensional intrinsically ferromagnetic semiconductor CrGeTe₃. *Phys. Rev. B* **95**, 245212 (2017).
- Wildes, A. R. et al. Anisotropy and the critical behaviour of the quasi-2D antiferromagnet, MnPS₃. *J. Magn. Magn. Mater.* **310**, 1221–1223 (2007).
- Wildes, A. R., Simonet, V., Ressouche, E., Ballou, R. & McIntyre, G. J. The magnetic properties and structure of the quasi-two-dimensional antiferromagnet CoPS₃. *J. Phys. Condens. Matter* **29**, 455801 (2017).
- Wildes, A. R. et al. Magnetic structure of the quasi-two-dimensional antiferromagnet NiPS₃. *Phys. Rev. B* **92**, 224408 (2015).
- Calder, S., Haglund, A. V., Kolesnikov, A. I. & Mandrus, D. Magnetic exchange interactions in the van der Waals layered antiferromagnet MnPSe₃. *Phys. Rev. B* **103**, 024414 (2021).
- Wildes, A. R. et al. Magnetic dynamics of NiPS₃. *Phys. Rev. B* **106**, 174422 (2022).
- Wiedenmann, A., Rossat-Mignod, J., Louisy, A., Brec, R. & Rouxel, J. Neutron diffraction study of the layered compounds MnPSe₃ and FePSe₃. *Solid State Commun.* **40**, 1067–1072 (1981).
- Ouvrard, G., Brec, R. & Rouxel, J. Structural determination of some MPS₃ layered phases (M = Mn, Fe, Co, Ni and Cd). *Mat. Res. Bull.* **20**, 1181–1189 (1985).
- Bhutani, A., Zuo, J. L., McAuliffe, R. D., de la Cruz, C. R. & Shoemaker, D. P. Strong anisotropy in the mixed antiferromagnetic system Mn_{1-x}Fe_xPS₃. *Phys. Rev. Mater.* **4**, 034411 (2020).
- Holstein, T. & Primakoff, H. Field dependence of the intrinsic domain magnetization of a ferromagnet. *Phys. Rev.* **58**, 1098 (1940).
- Wildes, A. R., Roessli, B., Lebeck, B. & Godfrey, K. W. Spin waves and the critical behaviour of the magnetization in MnPS₃. *J. Phys. Condens. Matter* **10**, 6417–6428 (1998).
- Leonel, S. A., Castro Oliveira, A., Costa, B. V. & Coura, P. Z. Comparative study between a two-dimensional anisotropic Heisenberg antiferromagnet with easy-axis single-ion anisotropy and one with easy-axis exchange anisotropy. *J. Magn. Magn. Mater.* **305**, 157–164 (2006).
- Wildes, A. R., Zhitomirsky, M. E., Ziman, T., Lançon, D. & Walker, H. C. Evidence for biquadratic exchange in the quasi-two-dimensional antiferromagnet FePS₃. *J. Appl. Phys.* **127**, 223903 (2020).
- Kartsev, A., Augustin, M., Evans, Richard F. L., Novoselov, K. S. & Santos, Elton J. G. Biquadratic exchange interactions in two-dimensional magnets. *npj Comput. Mater.* **6**, 150 (2020).
- Ni, J. Y. et al. Biquadratic exchange interactions in two-dimensional magnets. *Phys. Rev. Lett.* **127**, 247204 (2021).
- Zhao, J. et al. Spin waves and magnetic exchange interactions in CaFe₂As₂. *Nat. Phys.* **5**, 555 (2009).
- Liu, C., Lu, X., Dai, P., Yu, R. & Si, Q. Anisotropic magnetic excitations of a frustrated bilinear-biquadratic spin model: Implications for spin waves of detwinned iron pnictides. *Phys. Rev. B* **101**, 024510 (2020).
- Lee, S.-H. et al. Emergent excitations in a geometrically frustrated magnet. *Nature* **418**, 856–858 (2002).

40. Yao, W., Iida, K., Kamazawa, K. & Li, Y. Excitations in the ordered and paramagnetic states of honeycomb magnet $\text{Na}_2\text{Co}_2\text{TeO}_6$. *Phys. Rev. Lett.* **129**, 147202 (2022).
 41. Gao, B. et al. Diffusive excitonic bands from frustrated triangular sublattice in a singlet-ground-state system. *Nat. Commun.* **14**, 2051 (2023).
 42. Du, K. et al. Weak van der Waals stacking, wide-range band gap, and Raman study on ultrathin layers of metal phosphorus trichalcogenides. *ACS Nano* **10**, 1738–1743 (2015).
 43. Ye, F., Liu, Y., Whitfield, R., Osborn, R. & Rosenkranz, S. Implementation of cross correlation for energy discrimination on the time-of-flight spectrometer CORELLI. *J. Appl. Cryst.* **51**, 315–322 (2018).
 44. Petricek, V., Dusek, M. & Palatinus, L. Crystallographic computing system JANA2006: general features. *Z. Kristallogr.* **229**, 245–352 (2014).
 45. Abernathy, D. L. et al. Design and operation of the wide angular-range chopper spectrometer ARCS at the Spallation Neutron Source. *Rev. Sci. Instrum.* **83**, 015114 (2012).
 46. Azuah, R. T. et al. DAVE: a comprehensive software suite for the reduction, visualization, and analysis of low energy neutron spectroscopic data. *J. Res. Natl Inst. Stand. Technol.* **114**, 341 (2009).
 47. Toth, S. & Lake, B. Linear spin wave theory for single-Q incommensurate magnetic structures. *J. Phys. Condens. Matter* **27**, 166002 (2015).
- Project of Hangzhou Normal University (Grant no. 2020QDL026) and the Natural Science Foundation of Zhejiang Province (Grant no. LY22A040009). A portion of this research used resources at the Spallation Neutron Source, a DOE Office of Science User Facility operated by Oak Ridge National Laboratory.

Author contributions

L.C., J.-H.C., and P.D. initiated the project. L.C., X.T., and D.H. synthesized the FePSe_3 single-crystal samples. L.C., F.Y., G.E.G., and P.D. conducted the neutron scattering experiments. L.C. and P.D. performed data analysis. The manuscript was written by L.C. J.-H.C., R.J.B., and P.D. with inputs from all co-authors.

Competing interests

The authors declare no competing interests.

Additional information

Supplementary information The online version contains supplementary material available at

<https://doi.org/10.1038/s41535-024-00651-5>.

Correspondence and requests for materials should be addressed to Lebing Chen, Jae-Ho Chung, Robert J. Birgeneau or Pengcheng Dai.

Reprints and permissions information is available at <http://www.nature.com/reprints>

Publisher's note Springer Nature remains neutral with regard to jurisdictional claims in published maps and institutional affiliations.

Open Access This article is licensed under a Creative Commons Attribution 4.0 International License, which permits use, sharing, adaptation, distribution and reproduction in any medium or format, as long as you give appropriate credit to the original author(s) and the source, provide a link to the Creative Commons licence, and indicate if changes were made. The images or other third party material in this article are included in the article's Creative Commons licence, unless indicated otherwise in a credit line to the material. If material is not included in the article's Creative Commons licence and your intended use is not permitted by statutory regulation or exceeds the permitted use, you will need to obtain permission directly from the copyright holder. To view a copy of this licence, visit <http://creativecommons.org/licenses/by/4.0/>.

Acknowledgements

The work at the University of California, Berkeley was supported by the U.S. DOE under contract no. DE-AC02-05-CH11231 within the Quantum Materials Program (KC2202) (R.J.B.). The neutron scattering and single-crystal synthesis work at Rice was supported by US NSF-DMR-2100741, NSF-DMR-2418154 (P.D.) and by the Robert A. Welch Foundation under grant no. C-1839 (P.D.), respectively. A part of this research is supported by the Edinburgh-Rice Strategic Collaboration Award (P.D.). X.T. and M.Y. are supported by the Gordon and Betty Moore Foundation's EPIQS Initiative through grant No. GBMF9470 and the Robert A. Welch Foundation Grant No. C-2175. The work of J.-H.C. was supported by the National Research Foundation (NRF) of Korea (Grant nos. 2020R1A5A1016518 and 2022R1F1A1074321). The research at Hangzhou Normal University is supported by The Open Project of Guangdong Provincial Key Laboratory of Magnetoelectric Physics and Devices, no. 2022B1212010008, Startup

© The Author(s) 2024